# THE APPROACH OF COUPLED REACTION CHANNELS TO $^{7}$Li + $^{11}$B SCATTERING

A.A. RUDCHIK, A.T. RUDCHIK, O.A. PONKRATENKO, K.W. KEMPER[1]

Institute for Nuclear Research, Nat. Acad. Sci. of Ukraine
*(47, Nauky Prosp., Kyiv 03680, Ukraine; e-mail: rudchik@kinr.kiev.ua),*

[1]Florida State University
*(Tallahassee, Florida 32306, USA; e-mail: kirby@martech.fsu.edu)*

UDC 539.171/539.172


The data on the $^{7}$Li + $^{11}$B elastic and inelastic scatterings at the energy $E_{\rm lab}(^{7}{\rm Li}) = 34$ MeV are analyzed within the method of coupled reaction channels (CRC). The deformation parameters of $^{7}$Li and $^{11}$B and the $^{7}{\rm Li}^{(*)} + {}^{11}{\rm B}^{(*)}$ optical model (OM) potential parameters are deduced, and the energy dependence of the optical model potential for the $^{7}{\rm Li}^{*} + {}^{11}$B and $^{7}$Li + $^{11}{\rm B}^{*}$ channels is obtained.

## 1. Introduction

Elastic and inelastic scatterings play a particular role in nuclear reactions due to their presence and dominance among other nuclear processes in nuclear collisions and their strong influence on other reaction channels. In the present state of the theory of nuclear reactions, the elastic scattering data are used as a base for the deduction of the OM potentials used in the studies of reactions.

At present, there is a tremendous interest in the use of direct nuclear reactions for the study of short-lived and exotic nuclei. In this case, the experimental data on reactions are analyzed within the CRC method. The OM parameters obtained from the scattering data are used for the entrance reaction channel. The OM parameters for a channel with exotic nucleus are fitted when it is not possible to carry out the scattering experimentally. This method can also be used to study the interaction of nuclei in their excited states. The corresponding OM parameters can be quite different from those for the ground-state scattering.

In this work, the $^{7}$Li + $^{11}$B elastic and inelastic scatterings are studied as a first step for the systematic investigation of the $^{7}$Li($^{11}$B, X) reactions used for the study of the OM potentials for $^{10}$Be + $^{8}$Be, $^{10}$B + $^{8}$Li, and other channels.

The data on the $^{7}$Li + $^{11}$B elastic and inelastic scatterings are available only at the energy $E_{\rm lab}(^{7}{\rm Li}) = 34$ MeV [1,2]. In [2], these data were analyzed within the method of coupled channels (CC) except for the angular distributions for the 7.286-MeV ($5/2^{+}$) and 8.92-MeV ($5/2^{-}$) excited states of $^{11}$B. In the present work, the data are analyzed also for these excited states of $^{11}$B. A new approach in the CRC-analysis was carried out: 1) one- and two-step transfer contributions to the scattering channels were investigated; 2) the energy-dependent OM parameters are used in the inelastic scattering channels that are important for high-energy excitations; 3) taking into account the Pauli principle, the radius $R_{\rm comp}$ of the $^{18}{\rm O} \to {}^{7}{\rm Li} + {}^{11}{\rm B}$ compound-nucleus was used as a lower value for the radius $R_V$ of the Woods—Saxon OM potential: $R_{\rm comp} < R_V$; 4) strong transitions to the excited states of $^{7}$Li and $^{11}$B were included in the CRC-analysis.

## 2. Main Statements and Relations of the Analysis of Data

The OM potentials of the Woods—Saxon type,

$$U(r) = V_0 f(r, R_V, a_V) + iW_S f(r, R_W, a_W), \qquad (1)$$

and the Coulomb potential of a uniformly charged sphere,

$$V_{\rm C}(r) = \begin{cases} b\frac{Z_P Z_T}{R_C}\left(3 - \frac{r^2}{R_C^2}\right), & r \le R_C \\ b\frac{2Z_P Z_T}{r}, & r > R_C \end{cases} \qquad (2)$$

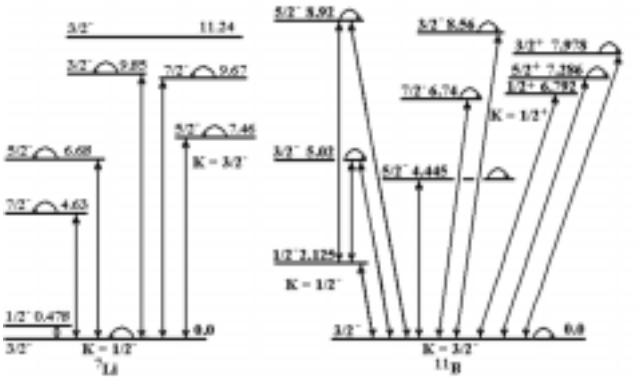

Fig. 1. Schemes of transitions to the excited states of $^{7}$Li and $^{11}$B

($b = 0.719862$), are used in the OM- and CRC-calculations for both the entrance and exit channels of the $^{11}$B+ $^{7}$Li elastic and inelastic scatterings. In (1),

$$f(r, R_i, a_i) = \left[1 + \exp\left(\frac{r - R_i}{a_i}\right)\right]^{-1}, \quad (3)$$

$$R_i = r_i(A_P^{1/3} + A_T^{1/3}),\ i = V, W, C, \quad (4)$$

$Z_P$, $A_P$ and $Z_T$, $A_T$ are the charge and mass numbers of a projectile (or ejectile) and a target (or target product), respectively.

The radius of the Coulomb potential for the entrance and exit channels was fixed at the value of $r_C = 1.25$ fm. The parameters $X = \{X_i\} = \{V_0, r_V, a_V, W_S, r_W, a_W\}$ were fitted within the optical model to obtain a good description of the elastic scattering data for $\theta_{c.m} < 90°$. The deduced optimal set $X_{opt}$ of the OM parameters was used as an initial one in the CRC-calculations. For the elastic scattering channel, only the parameter $W_S$ was fitted in these calculations. All OM parameters $\{X_i\}$ for the exit inelastic scattering channels were fitted because these OM parameters can differ from those of the elastic scattering channel due to the strong energy dependence of the OM parameters at the energies $E_{c.m} < 30$ MeV.

In the fitting procedure of the OM parameters, we took into account that the distance $R_V$ between the colliding nuclei $A_P + A_T$ cannot be smaller than the radius $R_{comp}$ of the corresponding compound nucleus due to the Pauli principle. Thus,

$$R_{comp} \approx 1.25(A_P + A_T)^{1/3} \leq R_V = r_V(A_P^{1/3} + A_T^{1/3}) \quad (5)$$

and

$$r_V \geq 1.25(A_P + A_T)^{1/3}/(A_P^{1/3} + A_T^{1/3}). \quad (6)$$

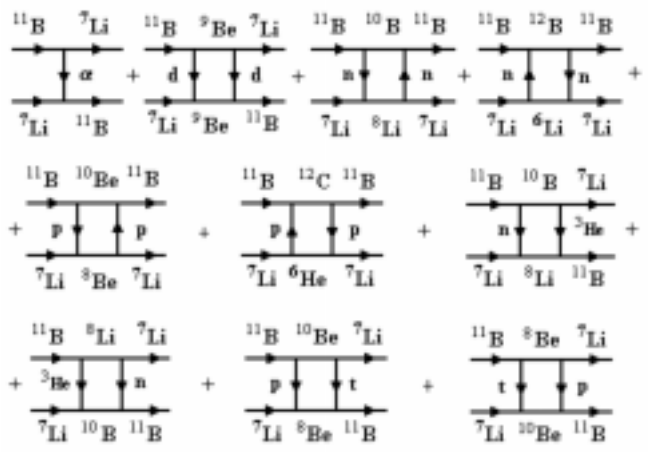

Fig. 2. Diagrams of one- and two-step transfers for $^{7}$Li + $^{11}$B scattering

According to this relation, the parameter $r_V \geq 0.792$ fm for the $^{7}$Li + $^{11}$B scattering.

We limited also the parameter $a_W$ by the relation $a_W \leq a_V$ to guarantee that

$$W(r) = W_S f(r, R_W, a_W) \leq V(r) = V f(r, R_V, a_V) \quad (7)$$

at any value $r$ in accordance with the statement that inelastic nuclear processes cannot occur without corresponding elastic scattering. This statement limited also the parameter $r_W$. We used only those values of the parameters $W_S$, $a_W$, and $r_W$ that fulfill relation (7).

The OM-calculations and the fitting of OM parameters for the elastic scattering were performed with the code SPI-GENOA [4].

In the CRC-analysis, the transitions to the $^{7}$Li and $^{11}$B excited states of a large energy range (up to 9.85 MeV) were included in the CC-scheme. Fig. 1 shows these transitions. The reorientations of $^{7}$Li and $^{11}$B in the ground and excited states are marked by the arcs.

We consider that the rotations of deformed $^{7}$Li and $^{11}$B nuclei play important roles in their low-energy excitations. The form-factor

$$V_\lambda(r) = -\delta_\lambda \frac{dU(r)}{dr}, \quad (8)$$

where $\delta_\lambda$ is the deformation length of the $\lambda$-multipole, was used in the CRC-calculations.

The deformation parameters used in the CRC-calculations are listed in Table 1.

The reorientation is considered as a quadrupole transition

$$\langle E, J^\pi | V_\lambda | E, J^\pi \rangle. \quad (9)$$

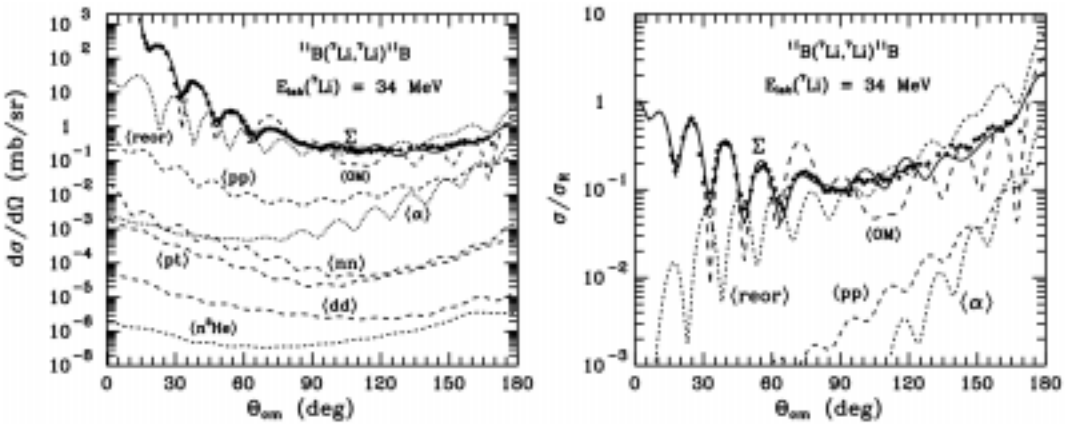


Fig. 3. Angular distribution of $^7$Li + $^{11}$B elastic scattering at $E_{\rm lab}(^7{\rm Li})$ = 34 MeV [1, 2] in absolute units (left panel) and in relation to the Coulomb scattering (right panel). The curves show the OM (curves $\langle OM\rangle$) and CRC angular distributions

We studied the contributions of one- and two-step transfers to the $^7$Li + $^{11}$B elastic and inelastic scattering data. The corresponding diagrams of these transfers are shown in Fig. 2. The most important transfers were included in the CC-scheme.

The spectroscopic amplitudes needed for the CRC calculations including transfer reactions were calculated within the translationary invariant shell model (TISM)[5] with the help of the code DESNA [6, 7] and the wave function tables [8]. These amplitudes $S_x$ of clusters $x$ in the systems $A = C + x$ are listed in Table 2 ($nL_j$ are the quantum numbers for the relative motion of cluster $x$ and core $C$).

**T a b l e 1. Transition multipoles and deformation parameters of $^7$Li and $^{11}$B ($\beta_\lambda$ for $R = 1.25A^{1/3}$ fm)**

| Nuclei | $E_x$, MeV | $J^\pi$ | $\Lambda$ | $\delta_\Lambda$, fm | $\beta_\Lambda$ | Ref. |
|---|---|---|---|---|---|---|
| $^7$Li | 0.0 | $3/2^-$ | 2 | 2.0 | 0.84 | [2] |
| | 0.478 | $1/2^-$ | 2 | 2.0 | 0.84 | [2] |
| | 4.630 | $7/2^-$ | 2 | 2.0 | 0.84 | |
| | | | 4 | 1.0 | 0.42 | |
| | 6.680 | $5/2^-$ | 2 | 2.0 | 0.84 | |
| | | | 4 | 1.0 | 0.42 | |
| | 7.460 | $5/2^-$ | 2 | 2.0 | 0.84 | |
| | | | 4 | 1.0 | 0.42 | |
| | 9.670 | $7/2^-$ | 2 | 2.0 | 0.84 | |
| | | | 4 | 1.0 | 0.42 | |
| | 9.850 | $3/2^-$ | 2 | 2.0 | 0.84 | |
| $^{11}$B | 2.125 | $1/2^-$ | 2 | 1.2 | 0.43 | [3] |
| | 4.445 | $5/2^-$ | 2 | 1.2 | 0.43 | [3] |
| | | | 4 | 1.0 | 0.36 | [3] |
| | 5.020 | $3/2^-$ | 2 | 1.2 | 0.43 | [3] |
| | 6.743 | $7/2^-$ | 2 | 1.2 | 0.43 | [3] |
| | | | 4 | 1.0 | 0.36 | [3] |
| | 6.792 | $1/2^+$ | 1 | 1.0 | 0.36 | [3] |
| | 7.286 | $5/2^+$ | 1 | 1.0 | 0.36 | [3] |
| | | | 3 | 1.2 | 0.43 | [3] |
| | 7.978 | $3/2^+$ | 1 | 1.0 | 0.36 | [3] |
| | | | 3 | 1.2 | 0.43 | [3] |
| | 8.560 | $3/2^-$ | 2 | 1.8 | 0.65 | [3] |
| | 8.920 | $5/2^-$ | 2 | 1.2 | 0.43 | |
| | | | 4 | 1.0 | 0.36 | |

The bound cluster wave function was calculated by the standard fitting method of the depth $V$ of a real Woods-Saxon potential to the cluster binding energy at the parameters $a$ = 0.65 MeV and $r_V = 1.25A^{1/3}/(C^{1/3} + x^{1/3})$.

The CRC-calculations were performed with the code FRESCO [9].

## 3. Elastic Scattering

First, the $^7$Li + $^{11}$B elastic scattering data at $E_{\rm lab}(^7{\rm Li})$ = 34 MeV ($E_{\rm c.m}$ = 20.78 MeV) [1, 2] were analyzed within the optical model. The set of the OM parameters $X = \{X_i\} = \{V_0, r_V, a_V, W_S, r_W, a_W\}$ was fitted to obtain the best description of the data for $\theta_{\rm c.m} < 90°$. The limitations of the OM parameters mentioned above, were taken into account. The obtained optimal set of the OM parameters $\{X_i\}$ is given in Table 2. The corresponding OM angular distribution is shown in Fig. 3 in absolute units (curve $\langle$OM$\rangle$ in the left panel) and in relation to the Coulomb scattering (right panel). One can see that the optical model fails in the description of the data at large angles. Then the CRC-approach was used to describe the data satisfactorily in the full angular range.

The optimal set of the OM parameters obtained in the fitting procedure was used in the CRC-calculations of the angular distributions for different transfers contributing to the $^7$Li + $^{11}$B elastic scattering data. Fig. 3 shows the CRC angular distributions for the transfers of an $\alpha$-cluster (curve $\langle\alpha\rangle$), p + p with two intermediate

**T a b l e 2. Spectroscopic amplitudes $S_x$ of $x$-clusters in $A = C + x$ systems**

| $A$ | $C$ | $x$ | $nL_j$ | $S_x$ | $A$ | $C$ | $x$ | $nL_j$ | $S_x$ |
|---|---|---|---|---|---|---|---|---|---|
| $^{7}$Li | $^{6}$He | p | $1P_{3/2}$ | 0.805 | $^{11}$B$^{*}_{4.445}$ | $^{7}$Li | $\alpha$ | $2D_2$ | $-0.049^{a}$ |
| $^{7}$Li$^{*}_{0.478}$ | $^{6}$He | p | $1P_{1/2}$ | 0.805 | | | | $1G_4$ | $-0.192^{a}$ |
| $^{7}$Li | $^{6}$Li | n | $1P_{1/2}$ | $-0.657$ | $^{11}$B$^{*}_{5.020}$ | $^{7}$Li | $\alpha$ | $3S_0$ | $-0.638$ |
| | | | $1P_{3/2}$ | $-0.735^{a}$ | | | | $2D_2$ | $-0.422$ |
| $^{8}$Li | $^{7}$Li | n | $1P_{1/2}$ | 0.478 | $^{11}$B$^{*}_{6.743}$ | $^{7}$Li | $\alpha$ | $2D_2$ | 0.104 |
| $^{8}$Be | $^{7}$Li | p | $1P_{3/2}$ | $1.234^{a}$ | | | | $1G_4$ | 0.124 |
| $^{8}$Be | $^{7}$Li$^{*}_{0.478}$ | p | $1P_{1/2}$ | $0.873^{a}$ | $^{11}$B$^{*}_{6.793}$ | $^{7}$Li | $\alpha$ | $2D_2$ | $0.596^{a}$ |
| $^{9}$Be | $^{7}$Li | d | $2S_1$ | $-0.226^{a}$ | $^{11}$B$^{*}_{7.286}$ | $^{7}$Li | $\alpha$ | $2D_2$ | $-0.049^{a}$ |
| | | | $1D_1$ | $0.111^{a}$ | | | | $1G_4$ | $-0.192^{a}$ |
| | | | $1D_3$ | $-0.624^{a}$ | $^{11}$B | $^{8}$Li | $^{3}$He | $1P_{1/2}$ | $0.160^{a}$ |
| $^{10}$Be | $^{7}$Li | t | $2P_{3/2}$ | $0.392^{a}$ | | | | $1F_{5/2}$ | $0.218^{a}$ |
| $^{10}$B | $^{7}$Li | $^{3}$He | $1P_{3/2}$ | 0.419 | | | | $1F_{7/2}$ | 0.214 |
| | | | $1F_{5/2}$ | $-0.104^{a}$ | $^{11}$B | $^{8}$Be | t | $2P_{3/2}$ | 0.641 |
| | | | $1F_{7/2}$ | 0.347 | $^{11}$B | $^{9}$Be | d | $2S_1$ | $-0.607^{a}$ |
| $^{11}$B | $^{7}$Li | $\alpha$ | $3S_0$ | $-0.638$ | | | | $1D_1$ | $-0.109^{a}$ |
| | | | $2D_2$ | $-0.422$ | | | | $1D_3$ | $0.610^{a}$ |
| $^{11}$B | $^{7}$Li$^{*}_{0.478}$ | $\alpha$ | $2D_2$ | $-0.422^{a}$ | $^{11}$B | $^{10}$Be | p | $1P_{3/2}$ | 0.699 |
| $^{11}$B | $^{7}$Li$^{*}_{4.63}$ | $\alpha$ | $2D_2$ | 0.362 | $^{11}$B$^{*}_{2.125}$ | $^{10}$Be | p | $1P_{1/2}$ | 0.699 |
| | | | $1G_4$ | 0.429 | $^{11}$B | $^{10}$B | n | $1P_{3/2}$ | $-1.347^{a}$ |
| $^{11}$B | $^{7}$Li$^{*}_{6.68}$ | $\alpha$ | $2D_2$ | $0.148^{a}$ | $^{12}$B | $^{11}$B | n | $1P_{1/2}$ | $-0.142^{a}$ |
| | | | $1G_4$ | $0.575^{a}$ | | | | $1P_{3/2}$ | $-0.127$ |
| $^{11}$B | $^{7}$Li$^{*}_{9.67}$ | $\alpha$ | $2D_2$ | 0.362 | $^{12}$C | $^{11}$B | p | $1P_{3/2}$ | $-1.706^{a}$ |
| | | | $1G_4$ | 0.429 | $^{12}$C | $^{11}$B$^{*}_{2.125}$ | p | $1P_{1/2}$ | $-1.206^{a}$ |
| $^{11}$B | $^{7}$Li$^{*}_{9.85}$ | $\alpha$ | $3S_0$ | $-0.638$ | $^{12}$C | $^{11}$B$^{*}_{5.021}$ | p | $1P_{3/2}$ | $-1.706^{a}$ |
| | | | $2D_2$ | $-0.422$ | $^{12}$C | $^{11}$B$^{*}_{6.793}$ | p | $1P_{1/2}$ | $-1.206^{a}$ |
| $^{11}$B$^{*}_{2.125}$ | $^{7}$Li | $\alpha$ | $2D_2$ | $0.596^{a}$ | | | | | |

$^{a}$ $S_{FRESCO} = (-1)^{J_C + j - J_A} S_x = -S_x$

**T a b l e 3. Parameters of the Woods—Saxon OM potentials**

| Channels | $E_{\mathrm{c.m}}$ MeV | $V$, MeV | $4_V$, fm | $a_V$, fm | $W_s$, MeV | $r_W$, fm | $a_W$ fm |
|---|---|---|---|---|---|---|---|
| $^{7}$Li$^{*}_{9.850}$ + $^{11}$B | 10.93 | 138.5 | 0.815 | 0.614 | 7.7 | 1.288 | 0.574 |
| $^{7}$Li$^{*}_{9.670}$ + $^{11}$B | 11.11 | 140.9 | 0.813 | 0.616 | 7.8 | 1.284 | 0.576 |
| $^{7}$Li + $^{11}$B$^{*}_{8.920}$ | 11.86 | 150.6 | 0.806 | 0.624 | 8.0 | 1.274 | 0.586 |
| $^{7}$Li + $^{11}$B$^{*}_{8.560}$ | 12.22 | 154.9 | 0.803 | 0.628 | 8.2 | 1.270 | 0.590 |
| $^{7}$Li + $^{11}$B$^{*}_{7.978}$ | 12.80 | 161.6 | 0.800 | 0.634 | 8.4 | 1.264 | 0.597 |
| $^{7}$Li$^{*}_{7.467}$ + $^{11}$B | 13.31 | 167.1 | 0.798 | 0.639 | 8.7 | 1.261 | 0.603 |
| $^{7}$Li + $^{11}$B$^{*}_{7.286}$ | 13.49 | 168.9 | 0.797 | 0.641 | 5.8 | 1.260 | 0.604 |
| $^{7}$Li + $^{11}$B$^{*}_{6.793}$ | 13.98 | 173.6 | 0.796 | 0.645 | 9.0 | 1.257 | 0.609 |
| $^{7}$Li + $^{11}$B$^{*}_{6.743}$ | 14.03 | 174.0 | 0.796 | 0.645 | 9.0 | 1.257 | 0.610 |
| $^{7}$Li$^{*}_{6.680}$ + $^{11}$B | 14.10 | 174.6 | 0.795 | 0.646 | 9.1 | 1.257 | 0.611 |
| $^{7}$Li + $^{11}$B$^{*}_{5.021}$ | 15.76 | 186.5 | 0.793 | 0.658 | 5.5 | 1.252 | 0.625 |
| $^{7}$Li$^{*}_{4.630}$ + $^{11}$B | 16.15 | 188.3 | 0.793 | 0.660 | 10.0 | 1.252 | 0.627 |
| $^{7}$Li + $^{11}$B$^{*}_{4.445}$ | 16.33 | 189.1 | 0.793 | 0.661 | 6.5 | 1.252 | 0.628 |
| $^{7}$Li + $^{11}$B$^{*}_{2.125}$ | 18.65 | 189.4 | 0.792 | 0.671 | 10.7 | 1.250 | 0.639 |
| $^{7}$Li$^{*}_{0.478}$ + $^{11}$B | 20.30 | 189.2 | 0.792 | 0.674 | 10.9 | 1.250 | 0.644 |
| $^{7}$Li + $^{11}$B | 20.78 | 189.2 | 0.792 | 0.674 | 10.2 | 1.250 | 0.644 |

channels (curve $\langle pp \rangle$), n + n with two intermediate channels (curve $\langle nn \rangle$), p + t and t + p (curve $\langle pt \rangle$), d + d (curve $\langle dd \rangle$), n + $^{3}$He and $^{3}$He + n (curve $\langle n^{3}\mathrm{He} \rangle$) and reorientations of $^{7}$Li and $^{11}$B (curve $\langle reor \rangle$). As one can see, the reorientations of $^{7}$Li and $^{11}$B dominate at large angles. The two-step proton and $\alpha$-cluster transfers dominate among other transfers. They give a small contribution to the data only at large angles. In Fig. 3, the solid curve $\Sigma$ shows the coherent sum of the potential scattering, reorientation processes, and the $\alpha$-cluster and two-step proton transfers. This CRC angular distribution describes the $^{7}$Li + $^{11}$B elastic scattering data satisfactorily.

## 4. Inelastic Scattering

The angular distribution of the $^{7}$Li + $^{11}$B inelastic scattering at the energy $E_{\mathrm{lab}}(^{7}\mathrm{Li}) = 34$ MeV [1] for the transition to the 0.478-MeV ($1/2^{-}$) state of $^{7}$Li is shown in Fig. 4. The curves represent the CRC angular distributions of the rotational transition $3/2^{-} \to 1/2^{-}$ for the $K = 1/2$ band (dotted curve $\langle rot \rangle$), sequential proton transfers through the intermediate channels of $^{8}$Be + $^{10}$Be and $^{6}$He + $^{12}$C (curve $\langle pp \rangle$) and $\alpha$-cluster transfer (curve $\langle \alpha \rangle$). The OM parameters for the $^{7}$Li$^{*}_{0.478}$ + $^{11}$B exit scattering channel were fitted to the data. The optimal set of the OM parameters is listed in Table 3.

Fig. 4 shows that the rotational transition dominates. The proton and $\alpha$-cluster transfers give small contributions to the data. As in the case of the $^7$Li + $^{11}$B elastic scattering, the contribution of other transfers (see the corresponding diagrams in Fig. 2) to the $^7\mathrm{Li}^*_{0.478}$ + $^{11}$B data is negligible. The coherent sum of above processes (solid curve) describes the $^7\mathrm{Li}^*_{0.478}$ + $^{11}$B data rather satisfactorily, except for the large-angle data.

Fig. 5 shows the angular distributions of the $^7$Li + $^{11}$B$^*$ inelastic scattering at the energy $E_{\mathrm{lab}}(^7\mathrm{Li})$ = 34 MeV [1] for excitations of 2.125-MeV $(1/2^-)$, 4.445-MeV $(5/2^-)$, 5.021-MeV $(3/2^-)$, 6.743-MeV $(7/2^-)$ + 6.793-MeV $(1/2^+)$, 7.286-MeV $(5/2^+)$, and 8.920-MeV $(5/2^-)$ states in $^{11}$B. The curves represent the CRC angular distributions calculated with the deformations, spectroscopic amplitudes, and OM parameters listed in Tables 1—3, respectively. The OM parameters for the $^7$Li + $^{11}$B$^*$ channels were fitted. The best description of the $^7$Li + $^{11}$B$^*$ data by the CRC angular distributions was obtained by using transitions to the $^{11}$B rotation bands shown in Fig. 1.

The $^7$Li + $^{11}\mathrm{B}^*_{2.125}$ data for the excitation of the 2.125-MeV $(1/2^-)$ state in $^{11}$B are described rather satisfactorily by the rotational CRC angular distribution (dotted curve in Fig. 5) ($K = 1/2$). The contributions of the transfer reactions to the $^7$Li + $^{11}\mathrm{B}^*_{2.125}$ data are small (curves $\langle pp\rangle$ and $\langle\alpha\rangle$) at forward angles. The solid curve shows the coherent sums of the CRC cross sections for the rotational transition and transfers of p + p and an $\alpha$-cluster.

A similar situation is observed also for the excitation of the 4.445-MeV $(5/2^-)$ state in $^{11}$B. The rotational transition (dotted curve) ($K = 3/2$) dominates. The reaction contributions are negligible (curve $\langle\alpha\rangle$) at forward angles. The CRC angular distribution (solid curve) describes the angular slope of the $^7$Li + $^{11}\mathrm{B}^*_{4.445}$ data and the failures in the description of the oscillations. There is some angular shift between the theoretical and experimental distributions.

The data for the excitation of the 5.021-MeV $(3/2^-)$ state in $^{11}$B are explained rather satisfactorily by the rotational model (dotted curve). Some discrepancy is observed only in the angular range $\theta_{\mathrm{c.m}} \approx 50^\circ - 80^\circ$.

The data for excitation of the 6.743-MeV $(7/2^-)$ + 6.793-MeV $(1/2^+)$ states in $^{11}$B are described satisfactorily by the incoherent sum of the CRC angular distributions for the rotational transitions to these states (dotted curve). As in the above cases, the reaction contributions to the data of these transitions are negligible.

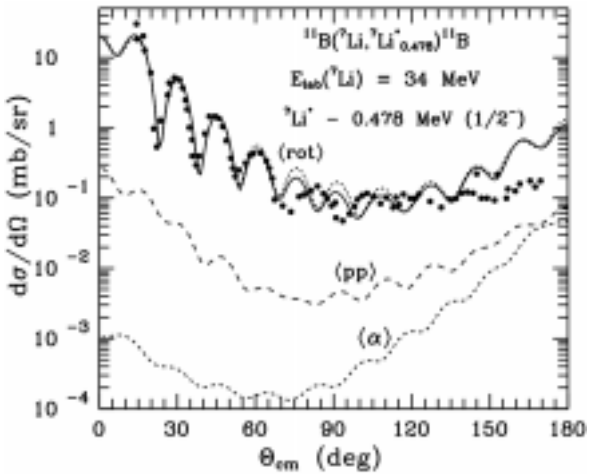


Fig. 4. Angular distribution of $^{11}\mathrm{B}(^7\mathrm{Li},^7\mathrm{Li}^*_{0.478})^{11}\mathrm{B}$ inelastic scattering at $E_{\mathrm{lab}}(^7\mathrm{Li})$ = 34 MeV [2] for the excitation of the 0.478-MeV $(1/2^-)$ state of $^7$Li. The curves represent the CRC angular distributions for the $^7$Li rotation (dotted curve $\langle rot\rangle$), proton transfer (curve $\langle pp\rangle$) and $\alpha$-cluster transfer (curve $\langle\alpha\rangle$). The solid curve shows the coherent sum of these processes

As Fig. 5 shows, the $^7$Li + $^{11}\mathrm{B}^*_{7.286}$ and $^7$Li + $^{11}\mathrm{B}^*_{8.920}$ data are also described satisfactorily within the CRC approach using the rotational model.

## 5. Energy Dependence of the OM Parameters

The energy dependences of the OM parameter sets $\{X_i\}$ = $\{V, W_S, r_V, r_W, a_V, a_W\}$ for the $^7$Li + $^{11}$B elastic and inelastic scattering at $E_{\mathrm{lab}}(^7\mathrm{Li})$ = 34 MeV [1] (see Table 3) are shown in Fig. 6 by dots.

We have [10]

$$X_i(E) = \begin{cases} X_i^{\max} - (X_i^{\max} - X_i^{\min})\; g(E, E_{X_i}, \Delta E_{X_i}) \\ \qquad \text{for} \quad X_i = V_0, W_S, a_v, a_w, \\ X_i^{\min} + (X_i^{\max} - X_i^{\min})\; g(E, E_{X_i}, \Delta E_{X_i}) \\ \qquad \text{for} \quad X_i = r_v, r_w, \end{cases} \tag{10}$$

$$g(E, E_{X_i}, \Delta E_{X_i}) = \left[1 + \exp\left(\frac{E - E_{X_i}}{\Delta E_{X_i}}\right)\right]^{-1}, \tag{11}$$

where $\{Y_i\} = \{\, X_i^{\min}, X_i^{\max}, E_{X_i}, \Delta E_{X_i}\}$ are the energy-dependent parameters and $E = E_{\mathrm{c.m}}$. The parameters $X_i^{\min}$ and $X_i^{\max}$ define the lower and upper limits of the OM parameter $X_i$, respectively. The parameter $E_{X_i}$ is the energy, at which $X_i(E_{X_i}) = (X_i^{\max} - X_i^{\min})/2$. The change of $X_i(E)$ near the point $E = E_{X_i}$ provides the parameter $\Delta E_{X_i}$.

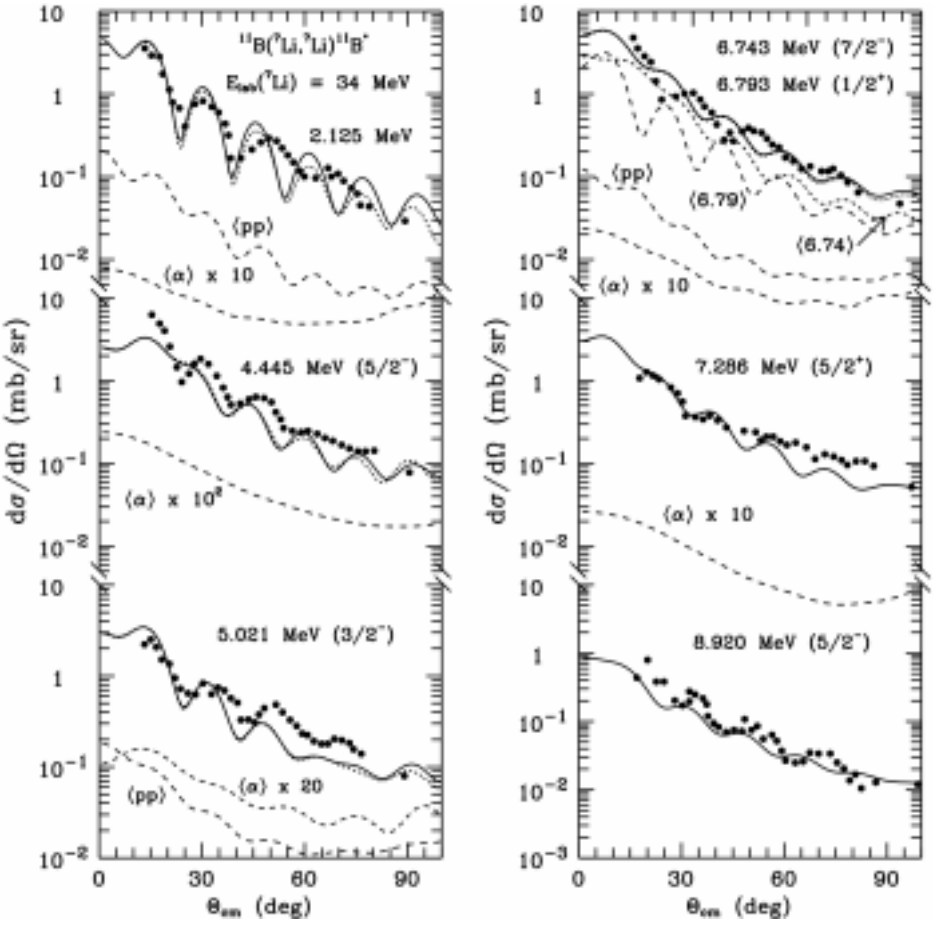


Fig. 5. Angular distribution of the $^{11}$B($^7$Li,$^7$Li)$^{11}$B$^*$ inelastic scattering at $E_{\rm lab}(^7{\rm Li}) = 34$ MeV [2] for the transition to the excited state of $^{11}$B. The curves represent the CRC angular distributions for the rotational transitions (dotted curves, dashed curves $\langle 6.74\rangle$ and $\langle 6.79\rangle$, solid curves for the 8.920-MeV state of $^{11}$B), $\alpha$-cluster transfer (curve $\langle\alpha\rangle$) and p + p-transfer (curve $\langle pp\rangle$). Solid curves show the sums of these processes

In addition to Eqs. (10) and (11), we used the dispersion relation between the real $V(r,E)$ and imaginary $W(r,E)$ parts of the OM potential [11]:

$$V(r,E) = V_0(r,E) + \Delta V_W(r,E), \qquad (12)$$

where

$$\Delta V_W(r,E) = \frac{\mathbf{P}}{\pi}\int_0^\infty \frac{W(r,E')}{E'-E}dE'. \qquad (13)$$

Here, **P** denotes the principal value of the integral. At $r = 0$, Eqs. (12) and (13) express the relation between the OM potentials $V_0$ and $W_S$.

The parameters $Y_i = X_i^{\rm min}$, $X_i^{\rm max}$, $E_{X_i}$ and $\Delta E_{X_i}$ were fitted to the OM parameters $X_i$ given in Table 3. As a result, the sets of the parameters $Y_i\} = X_i^{\rm min}$, $X_i^{\rm max}$, $E_{X_i}$, $\Delta E_{X_i}$ were deduced for the $^7$Li + $^{11}$B elastic and inelastic scatterings. These parameters are listed in Table 4. The corresponding energy dependences of the $^7{\rm Li}^{(*)}$ + $^{11}{\rm B}^{(*)}$ OM parameters are presented in Fig. 6 by the curves.

Fig. 6 shows that the parameter $W_S$ for the 4.445-MeV $(5/2^-)$, 5.021-MeV $(3/2^-)$, and 7.286-MeV $(5/2^-)$ states of $^{11}$B has smaller values (weak absorption) than its neighbors. This can be considered as a feature of the $^7{\rm Li}^{(*)}$ + $^{11}{\rm B}^{(*)}$ interaction in these excited states of $^{11}$B

**Table 4. Energy dependence of the $^7{\rm Li}^{(*)}$ + $^{11}{\rm B}^{(*)}$ OM parameters**

| $X_i$ / $Y_i$ | $V_0$, MeV | $W_S$, MeV | $r_V$, fm | $r_W$, fm | $a_V$, fm | $a_W$, fm |
|---|---|---|---|---|---|---|
| $X_i^{\rm min}$ | 59.9 | 7.0 | 0.792 | 1.250 | 0.553 | 0.500 |
| $X_i^{\rm max}$ | 289.9 | 11.1 | 0.900 | 1.405 | 0.679 | 0.649 |
| $E_{X_i}$, MeV | 9.9 | 14.1 | 9.000 | 9.145 | 11.139 | 10.984 |
| $\Delta_{X_i}$, MeV | 4.0 | 2.0 | 1.500 | 1.605 | 2.913 | 2.968 |

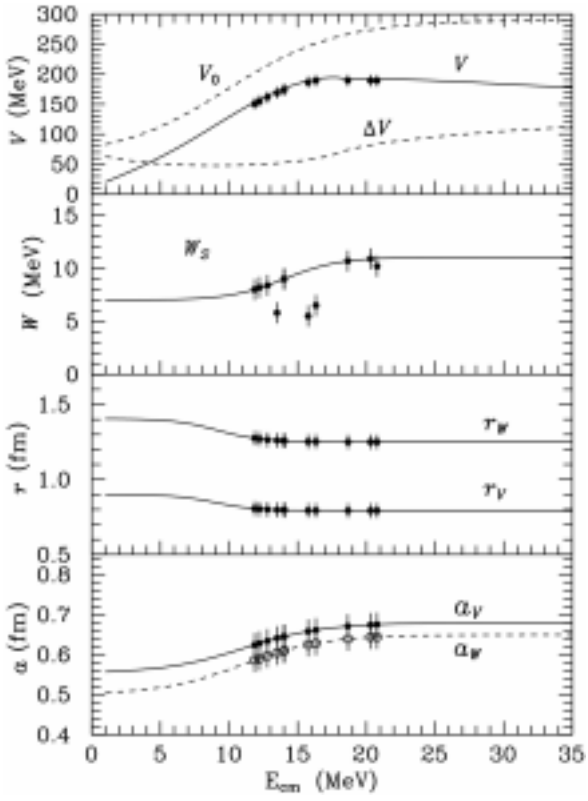


Fig. 6. Energy dependence of $^{7}Li^{(*)}$ + $^{11}B^{(*)}$ OM parameters

or as the additional contributions of other processes different from the rotation of $^{11}$B in these states. More precise conclusions can be obtained from the CRC analysis of the data at large angles which are sensitive to different types of transitions. Such data for the $^{7}$Li + $^{11}$B at the energy $E_{\rm lab}(^{11}{\rm B}) = 44$ MeV were obtained recently in the experiment at the Warsaw cyclotron C-200P [12].

## 6. Summary and Conclusions

The data on the $^{7}$Li + $^{11}$B elastic and inelastic scatterings at the energy $E_{\rm lab}(^{7}{\rm Li}) = 34$ MeV [1, 2] have been analyzed within the optical model and method of coupled reaction channels. The transitions to excited states are calculated by using the rotational model. The elastic and inelastic channels with the reorientations of $^{7}$Li and $^{11}$B as well as the strong particle transfers were included in the coupling scheme.

It is found that, in the $^{7}$Li + $^{11}$B elastic channel, the potential scattering and reorientations of $^{7}$Li and $^{11}$B dominate at forward and backward angles, respectively. The rotational transitions to the excited states of $^{7}$Li and $^{11}$B dominate in the inelastic channels. The contributions of one- and two-step transfers to the elastic and inelastic channels are small. The $\alpha$-cluster and sequential proton + proton transfers dominate among other transfers.

As a result of the present analysis, the $^{7}$Li + $^{11}$B OM parameters for the ground and excited states of $^{7}$Li and $^{11}$B as well as the deformation parameters of these nuclei are deduced. It is found that the OM parameter $W_S$ for the $^{7}$Li + $^{11}$B$^{*}$ channels with the 4.445-MeV ($5/2^{-}$), 5.021-MeV ($3/2^{-}$) and 7.286-MeV ($5/2^{-}$) states of $^{11}$B is smaller (weak absorption) as compared to other states of these nuclei. This is considered to be due to the significant contributions to these states from other types of transitions that differ from a pure rotation. To confirm this hypothesis, the large-angle data on the $^{7}$Li + $^{11}$B inelastic scattering for the transitions to these excited states of $^{11}$B are needed.

The energy dependence of the $^{7}$Li + $^{11}$B OM parameters for the ground and excited states of $^{7}$Li and $^{11}$B was obtained at the energies $E_{\rm c.m} \approx 12$—21 MeV.

One of us (K.W. Kemper) acknowledges the support of the U.S. National Science Foundation and NATO.

1. *Cook J., Stephens M.N., Kemper K.W.* // Nucl. Phys. A.— 1987.— **466**.—P.168—188.
2. *Cook J., Abdallah A.K., Stephens M.N., Kemper K.W.* // Phys. Rev. C.— 1987.— **35**.—P.126—136.
3. *Rudchik A.T., Kyryanchuk V.M., Budzanowski A. et al.* // Nucl. Phys. A.— 2003.—**714**.—P.391—411.
4. *Nilsson B.S.* // SPI-GENOA: an Optical Model Search Code.— A Niels Bohr Institute report, 1976.
5. *Smirnov Yu.F., Tchuvil'sky Yu.M.* // Phys. Rev. C.— 1977.— **15**.— P.84.
6. *Rudchik A.T., Tchuvil'sky Yu.M.* A code DESNA: Report KIYAI-82-12 of the Institute for Nuclear Research of the NASU.— Kyiv, 1982 (in Russian).
7. *Rudchik A.T., Tchuvil'sky Yu.M.* // Ukr. Fiz. Zh.— 1985.— **30**.— P.819.
8. *Boyarkina A.N.* // Structure of 1*p*-Shell Nuclei.— Moscow: Moscow University, 1973 (in Russian).
9. *Thompson I.J.* // Comp. Phys. Repts.— 1988.— **7**.—P.167—212.
10. *Rudchik A.T., Budzanowski A., Chernievsky V.K. et al.* // Nucl. Phys. A.— 2001.— **695**.— P.51—68.
11. *Mahaux C., Ngŏ H., Satchler G.R.* // Ibid.— 1986.— **449**.— P.354.
12. *Rudchik A.A., Rudchik A.T., Budzanowski A. et al.* // LIV Intern. Meet. on Nucl. Spec. and Nucl. Struc. "Nucleus-2004".— Belgorod, 2004.— P.180.

Received 21.10.04

ДОСЛІДЖЕННЯ РОЗСІЯННЯ ЯДЕР $^{7}$Li + $^{11}$B МЕТОДОМ ЗВ'ЯЗАНИХ КАНАЛІВ РЕАКЦІЙ

*А.А. Рудчик, А.Т. Рудчик, О.А. Понкратенко, К.В. Кемпер*

Р е з ю м е

Проаналізовано експериментальні дані пружного і непружного розсіяння ядер $^{7}$Li + $^{11}$B при енергії $E(^{7}\mathrm{Li}) = 34$ МеВ методом зв'язаних каналів реакцій. Отримано параметри деформації ядер $^{7}$Li та $^{11}$B, а також параметри оптичного потенціалу взаємодії ядер $^{7}\mathrm{Li}^{(*)} + {}^{11}\mathrm{B}^{(*)}$ в основних та збуджених станах. Досліджено енергетичну залежність параметрів оптичного потенціалу для каналів $^{7}\mathrm{Li}^{*} + {}^{11}$B і $^{7}$Li + $^{11}\mathrm{B}^{*}$.